Robust and hydrophilic polymeric films with honeycomb pattern and their cell scaffold applications

Lei Li,*[a] Caikang Chen,[a] Jian Li,[a] Aijuan Zhang,[a] Xinyu Liu,[a] Bin Xu,[b] Shubin Gao,[b] Guanghui Jin*[b] and Zhi Ma*[c]

Received 13th November 2008, Accepted 2nd February 2009
First published as an Advance Article on the web 9th March 2009
DOI: 10.1039/b820279f

Starting from a commercially available block copolymer, polystyrene-*b*-polybutadiene-*b*-polystyrene (SBS), micro-patterned polymer films were successfully prepared by evaporating SBS/carbon disulfide solutions with different concentrations under high humidity. The influence of solution concentration on the pore size and array was investigated in detail. With the increase of solution concentration, regular pore arrays turned into random because of weakened convention. Once the concentration was more than 60 mg mL^{-1}, a bimodal size distribution appeared. Photo-chemical cross-linking was achieved by exposing the polymer films in deep UV light (wavelength = 254 nm), monitored by attenuated total reflective Fourier transform infrared and X-ray photoelectron spectroscopy. After 1 h cross-linking, either solvent resistance or thermal stability or surface wettability of the films was significantly improved. The cross-linked honeycomb structured films became resistant to a wide range of organic solvents and thermally stable up to 350 °C, an increase of more than 250 K as compared to the un-crosslinked films. Another beneficial effect of the photo-chemical process was the formation of polar groups on the film surface, changing surface wettability from hydrophobicity to hydrophilicity, enhanced by the micro-patterned surface. The resultant films were non-cytotoxic and hence suitable as cell scaffolds. It was found that hydrophilic, micro-patterned polymer films with a uniform pore size of 3 μm facilitated cell attachment and proliferation.

Introduction

There is an intensifying interest in the use of micro-patterned biofunctional materials to organize and control the growth of cells on surfaces. Such materials offer attractive capabilities for cell-based biosensor technologies, microfluidic cell screening systems, tissue engineering applications and fundamental research. Both surface chemistry and substrate topographical features have a great effect on cell adhesion and spreading. Many strategies have been employed to modify substrate surfaces. One is to change the chemical composition to improve biocompatibility by introducing hydrophilic functional groups by ion-assisted reaction, plasma treatment, incorporating integrin receptor-binding peptides, molecular self-assembly and grafting.[1–4] The other one is to create micro- and nanostructures on substrate surfaces using such methods as electron-beam lithography, soft lithography, photolithography, interference lithography, colloidal lithography and nano-imprinting lithography.[5–8] The modification methods are, in fact, rather complicated, usually including several steps.

Polymers are widely used in cell culture applications because of their non-toxicity, high transparency and low production cost.[9] However, unmodified plastics surface cannot provide a suitable environment for cell growth because of the hydrophobicity. Many researchers have developed various kinds of methods to modify plastics surface in order to improve biocompatibility and convey new functional abilities such as antibacterial, selective adhesion and cell orientation properties. For example, Kim *et al.* employed an ion-assisted reaction to improve wettability and to supply a suitable PS surface for cell culturing.[10] Tsuji *et al.* reported the control of cell orientation by a negative-silver-ion implantation technique.[11] Groves *et al.* used phospholipid bilayers as biomimetic coating materials to modulate the adhesion and growth of cells on PS substrates.[12] Detrait *et al.* reported the orientation of cell adhesion on heterogeneous polystyrene surfaces composed of oxygen plasma-treated stripes.[13] Recknor *et al.* found that astrocytes or AHPCs cultured on chemically modified micro-patterned polystyrene substrates with laminin exhibited over 75% alignment in the groove direction.[14] However, as the above mentioned methods, chemical modification of the polymer surface usually needs rigorous conditions, complicated procedures or coating materials which are not easily accessible. Therefore, it still remains a challenge to develop simple and economical methods to modify the plastics surface physically and chemically. Additionally, in order to be used for the practical applications, the chemical and thermal stability of the porous films in harsh environment is required.

Recently, the formation of honeycomb structured polymeric films, prepared by a simple evaporation method of a water-immiscible polymer solution under high humidity, has sparked a wide interest in these fields.[15] In the so-called breath-figure method, water vapour is condensed onto the cooling surface

[a]*College of Materials, Xiamen University, Xiamen, 361005, P. R. China. E-mail: lilei@xmu.edu.cn; Fax: +86-592-2183937; Tel: +86-592-2186296*
[b]*Medical College, Xiamen University, Xiamen, 361005, P.R. China*
[c]*Shanghai Institute of Organic Chemistry, Chinese Academy of Sciences, Shanghai, 200032, P. R. China*

caused by rapid solvent evaporation, then the droplets are trapped into the solution surface by the surface tension. Condensed water droplets form hexagonal array induced by capillary force on the solution surface, and then, honeycomb structure is formed on the polymer film surface after evaporation of the solvent, without the need for expensive lithographic techniques. By changing the rate of air flow, the concentration of polymer solution and the humidity, micro-scale pores with different size and shape can be easily tailored. The surface wettability can be further modified by simple chemical or photochemical reactions. The resultant porous polymer films offer a variety of promising applications including protein array,[16] tissue-engineering and scaffold cell growth.[17,18]

Polystyrene-*b*-polybutadiene-*b*-polystyrene (SBS) is a commercially available block copolymer, which is believed to be an ideal candidate for the porous materials by breath-figure method.[19] Furthermore, either polystyrene (PS) or polybutadiene (PB) composition can be cross-linked and polarized conveniently by deep UV irradiation.[20] The photo-chemically cross-linked polymer films have improved thermal stability, solvent resistance and surface wettability, which are critical for the following applications. In this paper, we present a static breath-figure method to prepare ordered honeycomb SBS films. The pore size and film structure can be adjusted by simply changing the solution concentration. In the following UV irradiation, not only the porous structures are well preserved, but also thermal and chemical resistance of the films is significantly improved due to the cross-linkage. Both the attenuated total reflective Fourier transform infrared (ATR-FTIR) and X-ray photoelectron spectroscopy (XPS) spectra confirm the formation of polar groups on the film surface after irradiation. The surface wettability is changed from hydrophobicity to hydrophilicity. The cell attachment and spread are enhanced by the micro-patterned surface and increased hydrophilicity.

Experimental

Materials

A commercially available SBS sample was purchased from Asahi Company and used as received. All the chemical regents were used as received without further purification.

Preparation of honeycomb films

The glass substrates (0.5×1 cm^2) were cleaned by detergent and acetone successively and air dried. A static breath-figure process was operated in a 25 mL straight-mouth glass bottle with a cap. A saturated relative humidity in the vessel was achieved beforehand by adding 2 mL distilled water into the bottle. A piece of cleaned glass substrate was adhered on the top of a plastic stand with double sided tape and placed into the glass vessel. The glass substrate was 1 cm higher than the liquid level. Polymer solutions with different concentrations were prepared by dissolving SBS pellets in carbon disulfide (CS_2).

The micro-patterned film was prepared by casting 100 μL polymer solution onto the substrate with a microsyringe. With organic solvent volatilization, the transparent solution surface became turbid. The film was taken out for microscope observation after complete solvent evaporation. All the experiments were carried out at room temperature unless stated otherwise.

Photochemical cross-linking

The photochemical cross-linking was performed at 30 °C in a ZWLH-5 UVO cleaner (Tianjin, China) in the presence of air, by exposing the polymer films into UV light. The cleaner generated UV emissions at a wavelength of 254 nm and power of 500 W. The distance between the UV source and the film surface was 10 cm.

Thermal and solvent treatment

Thermal treatment was carried out in a hot stage (METTLER TOLED FP82HT) that was attached to an optical microscope (Olympus BH2) with a long range 40× objective lens. Solvent treatment was to immerse the polymer films into the organic solvents for one minute and then the film was air dried for microscope observation.

Characterization

The polymer films were coated with a thin layer of gold (around 2 nm) for imaging with a Philips XL20 scanning electron microscope (SEM). A 10 keV electron beam was used for the observation with a working distance of 10 mm in order to obtain secondary electron images.

ATR-FTIR spectra were obtained using a Nicolet Avatar 360 with a Ge window. All spectra (32 scans at a resolution of 4.0 cm^{-1}) were recorded at 25 °C and corrected for the atmospheric background spectra at fixed intervals from 680–4000 cm^{-1}.

XPS spectra were acquired with a PHI Quantum 2000 spectrometer using monochromated X-rays from an AlKα source with a take-off angle of 45° from the surface plane. The atomic fractions of carbon and oxygen were computed using the attenuation factors provided by the supplier and the sum of these atomic fractions was normalized to unity. The static contact angle (CA) was measured with a JC2000A optical contact angle equipment at room temperature.

Cell culture and EGFP gene transfection

The lung cancer cell line A549 was obtained from the American Tissue Collection Center (ATCC, Philadelphia, USA) and cultured in Dulbecco's modified Eagle's medium (DMEM) (Hyclone, Utah, USA) supplemented with 10% (v/v) fetal bovine serum (FBS), penicillin (100 U mL^{-1}) and streptomycin (100 μg mL^{-1}) at 37 °C in a 5% CO_2 atmosphere.

In order to get the fluorescence view, A549 cells were transfected with a plasmid, pEGFP-C1, by PEI method.[21] A549 cells were harvested and seeded in 10 cm cell culture dish with a density of 2×10^6 cells per dish, in which the substrates were fixed. The cell adherence and growth were observed by fluorescence microscope (Nikon, ECLIPSE, TE2000-U). For imaging, light from a xenon lamp passed through monochromator to provide excitation (485 nm) into the fluorescent port of an inverted Zeiss microscope equipped with a ×20 objective. The

cell growth on the substrate surface was expressed in terms of the number of attached cells per cm^2.

Results and discussion

Formation of honeycomb films

Although a variety of polymers have been used to prepare honeycomb structured films by breath-figure method, the pattern forming mechanism is not yet well understood. Different polymers require different preparation conditions, which makes the process more empirical. Breath-figure templating requires that the solute prevents water droplets coalescence. This requirement has been met by a wide range of colloidal materials, including star-shaped polymers and block copolymers because of their high segment density.[22] Additionally, a highly volatile, water-immiscible organic solvent, such as CS_2 or chlorinated solvents, is believed to be another prerequisite for the successful formation of honeycomb structured porous films.[19] The rapid solvent evaporation leads to a decrease in solution temperature and facilitates the condensation of water droplets on solution surface. In a dynamic atmosphere, the evaporation rate of solvent and humidity are adjustable by controlling air flow. The pore size and shape can be tailored by changing the flow rates, solution concentrations and humidities. In our case, a much simpler static method as mentioned in the Experimental Section is employed to fabricate micro-patterned films without the need of flowing gas and valve. The pore size and shape are tuned by changing the solution concentrations.

The influence of solution concentration on the formed microporous structures is investigated by SEM and demonstrated in Fig. 1. No clear patterns are formed on the film surface when the solution concentration less than 10 mg mL^{-1} (Fig. 1a). With increasing the concentration to 12 mg mL^{-1}, highly ordered holes separated by thin walls are formed in the whole film area (Fig. 1b). The associated fast Fourier transform (FFT) of the SEM image (right inset in Fig. 1b), with first- and high-order spots, shows the very regular character of the main structures. When the solution concentration ranging from 25–50 mg mL^{-1}, the pores turn into interconnected and slightly disordered, as demonstrated in Fig. 1c–d. Further increasing the solution concentration to 60 mg mL^{-1}, larger holes (around 10 μm) separated by thick walls are found predominantly in the film (Fig. 1e). A magnified SEM image (Fig. 1f) shows that satellite holes having smaller size (around 2 μm) appear on the walls, which causes an apparently bimodal size distribution. No long range order is found in the whole surface area. The similar bimodal size distribution persists in the micro-patterned films even casting from a solution with a higher concentration.

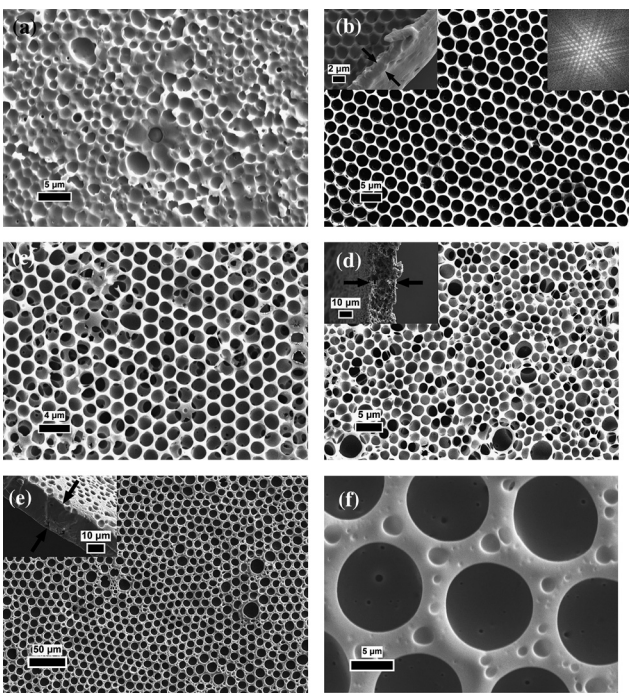

Fig. 1 Scanning electron micrographs of micro-patterns on the SBS film surfaces. The films are prepared by casting from SBS/CS_2 solutions with different concentrations. (a) 6 mg mL^{-1}; (b) 12 mg mL^{-1}; (c) 25 mg mL^{-1}; (d) 50 mg mL^{-1}; (e) 62 mg mL^{-1} and (f) a magnified area in (e).

The dependence of pore sizes on the solution concentrations is summarized and plotted in Fig. 2. Note that the bars do not represent the experimental errors but primarily the distribution of pore diameter. The average sizes of main structures and satellite pores are distinguished by open and filled squares, respectively. It is evident that the main structures, casting from low concentration solution, consist of pores having a uniform size of around 2 μm. The pore size decreases slightly with the increase of solution concentration. The bimodal size distribution appears when solution concentration more than 60 mg mL^{-1}. Additionally, the scale bar of either the satellite pores or main structures is wide, indicative of broad size distribution.

The influence of solution concentrations on the pore size is explained as follows. After placing a droplet of polymer solution on the substrate under a humid atmosphere, the solvent starts to evaporate. This leads to a decreased solution temperature, and then water droplets start to condense onto the air/polymer solution interface. During this process, the polymer dissolved in the solution is absorbed to the interface between the water and the polymer solution, which stabilizes the water droplets and prevents their coagulation. Periodic water droplets are packed and transported to the solution front by the convection flow or the capillary force. When all of the solvent has evaporated, the

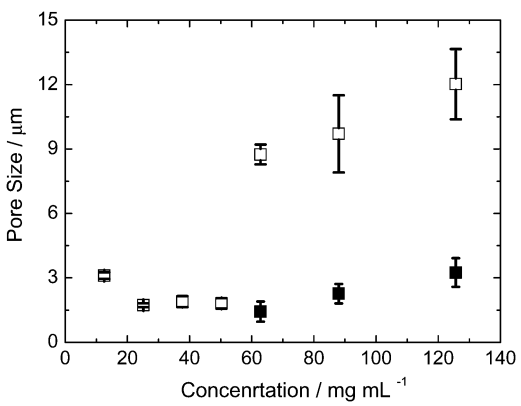

Fig. 2 Plot of the dependence of pore sizes on solution concentrations. Open squares: the average size of main structures in the films; filled squares: the average sizes of satellite pores.

film returns to ambient temperature, thus allowing the condensed water micro-droplets to subsequently evaporate, and leaving behind the observed microporous structure. Polymer precipitation is believed to be a key element in producing regular hole pattern.[23] When solution concentration is comparably low, the solution viscosity is too low to encapsulate the droplets or prevent their coalescence, resulting in the formation of disordered structures. With the increasing of solution concentration (solution viscosity), water droplets can be effectively trapped onto the solution surface so that highly ordered patterns appear (Fig. 1b). Say, casting from a 12 mg mL^{-1} polymer solution, the rapid evaporation of solvent results in the low temperature of solution surface. The formation of ordered patterns contributes to the convection generated in the evaporating solution and the lateral capillary force between the adjacent droplets (Marangoni effect). The cross-section SEM view shows that the film thickness is close to the pore diameter of 2 μm under this concentration (left inset in Fig. 1b), indicating that only single layer of water droplets is accommodated inside the film. The solvent in a more concentrated solution has a lower vapour pressure, which reduces the evaporation rate of solvent. A higher surface temperature is obtained due to the decrease of evaporation rate. The growth rate of droplets is proportional to the temperature difference (ΔT) between the atmosphere and the solution surface, which is described as $dR/dt \sim \Delta T^{0.8}$.[24] The lower growth rate of droplets is obtained due to the reduced temperature difference. In addition, the increased viscosity will weaken the convection in the solution, which is not beneficial to the ordered packing of droplets, so that the pore size is slightly reduced and the package of pores becomes disorder (Fig. 1c–e). Since the casting droplets have the same volume in each operation, the resultant films become thicker and thicker with the increased solution concentration. A film with a thickness more than 10 μm is formed after casting from a 50 mg mL^{-1} solution. Here, the condensed water droplets do not coalesce, but start to sink into the solution, propagate through the film and become interconnected. The inset in Fig. 1d definitely demonstrates the network structures and connectivity. When the concentration more than 60 mg mL^{-1}, the convection in the polymer solution is significantly reduced with the increased solution viscosity. It is difficult for the droplets to sink into the solution surface because of the high viscosity although a 15 μm film thickness can be achieved under this concentration (inset in Fig. 1e). The droplets float on the solution surface, so the coalescence occurs inevitably. The formation of large pores in random is attributed to the collision of the neighbouring droplets and the rapid solidification. The smaller satellite holes around the main structure are believed to be the uncollided droplets since they have an equivalent size to that in the films casting from low concentration solution.

Photochemical cross-linking and surface modification

In order to achieve their stability in harsh environment, the obtained honeycomb porous films should be effectively cross-linked. Thermal or chemical cross-linking will deform the obtained honeycomb structures. Photochemical cross-linking process is operated at room temperature and easy to control, suitable for the preservation of the porous structures in the films.[25,26] Recently, we reported that thermal stability of a polystyrene-*b*-poly(acrylic acid) block copolymer film with micro-patterns was significantly improved by simply UV cross-linking in air. It was found that the 3D honeycomb structures of the films could be preserved up to 320 °C after 6 h UV exposure, an increase of more than 200 K as compared to the un-crosslinked films.[27]

The photochemical process in PS and PB has been widely investigated.[20] It has been proved that either PS or PB was cross-linkable under deep UV irradiation in air, though the mechanism was controversial. Herein, the UV irradiation process is employed to cross-link PS and PB blocks in order to improve the thermal stability and chemical resistance of the micro-patterned films for the practical application.

The photo-chemical processes taking place in PS and PB upon exposure to deep UV irradiation in air are complicated, including cross-linking, chain scission and oxidation. The well-accepted cross-linking mechanisms of PS and PB compositions are shown in Scheme 1 and 2, respectively. For PS composition, by abstracting hydrogen atoms from polymer molecules, macro-radicals form during the irradiation. The movement of macro-molecules in the solid sate is restricted, but free radicals can migrate along the polymer chain until they are trapped by other free radicals or impurities. When two macro-radicals are near to each other cross-linking may occur. Alkoxy polymer radicals

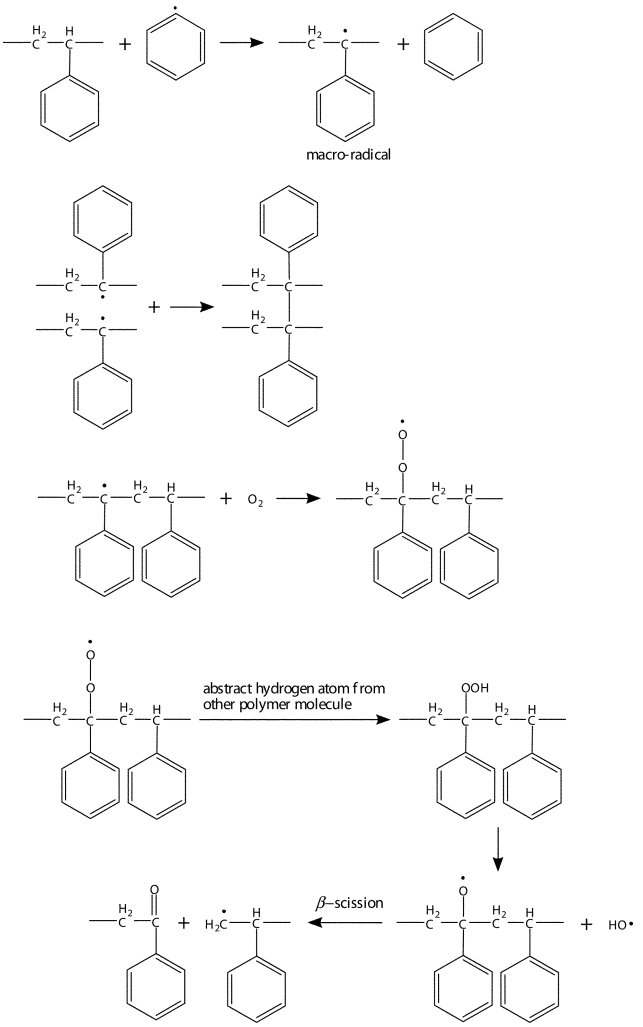

Scheme 1

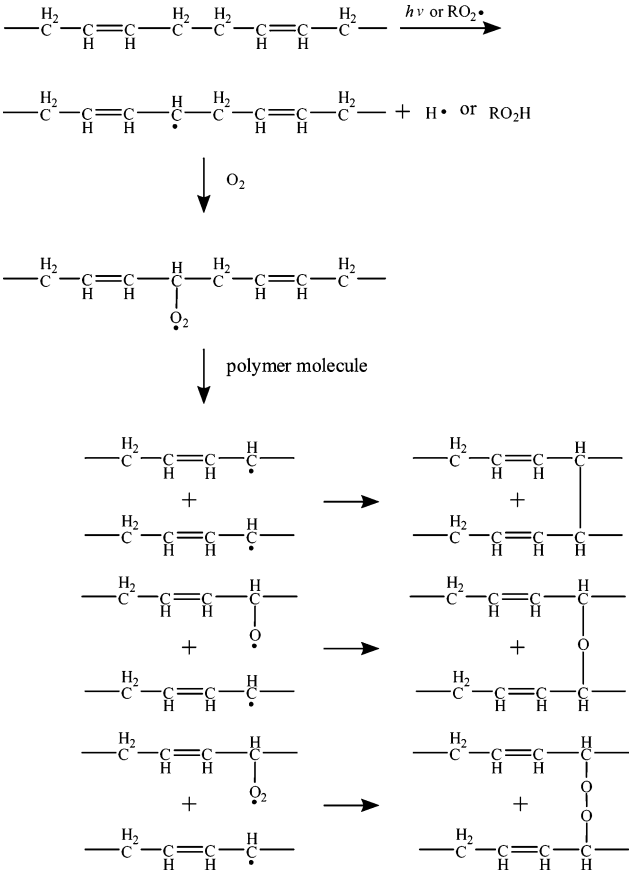

Scheme 2

produced during the photolysis of hydroperoxide groups may decompose by a β-scission and form carbonyl groups (Scheme 1). The photochemical reaction in PB composition, including cross-linkage and formation of polar group, is shown in Scheme 2. Initiated by light or a peroxy radical, the first stage involves the formation of polymer alkyl radical. The polymer alkyl radicals react with oxygen to give polymer peroxy radicals. Hydroperoxides are formed by reaction between polymer peroxy radicals and other polymer molecules, which can decompose to oxy and alkyl polymer radicals by the same process. Polymer alkyl radicals, alkoxy and peroxy radicals can react with each other to give the cross-linking structure in the polymer films. Cross-linking reaction not only affords the polymer films excellent thermal and chemical resistance, but also endows the film surface hydrophilicity by the introduced polar groups.

The photochemical reaction is monitored by ATR-FTIR and XPS. Fig. 3 shows the ATR-FTIR spectra of the SBS films before (solid line) and after (dash line) UV irradiation. In the spectrum of un-crosslinked film, the band at 3020 cm^{-1} is assigned to the stretching mode of the =C–H bonds, the bands at 2919 and 2849 cm^{-1} are identified as the asymmetric stretching of the C–H bonds in the CH_2 groups of the PS and PB chain, the band at 1450 cm^{-1} is assigned to the deformation mode of the CH_2 bonds in the PB chain, and the bands at 962 and 911 cm^{-1} are due to the bending mode of the C–H of the PB chain out of plane. After 1 h irradiation, the most significant difference in the spectra is the appearance of an intense and sharp band around 1720 cm^{-1} that

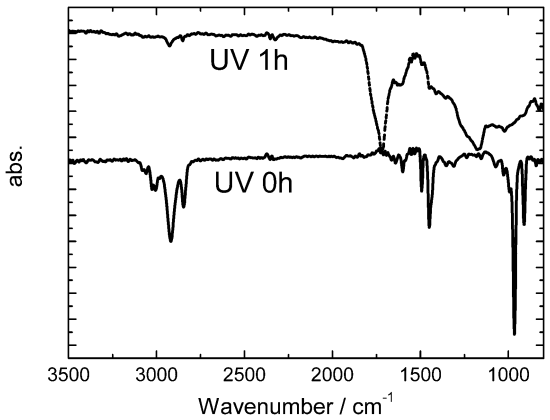

Fig. 3 ATR-FTIR spectra of the honeycomb structured films before (solid line) and after (dash line) cross-linking process.

can be attributed to the formation of carbonyl (–C=O) containing species. Another broad band centered at 1170 cm^{-1} is assigned to the formation of ether bond in PB composition during the UV irradiation.

Fig. 4a and b show the XPS spectra of un-crosslinked and crosslinked SBS films, respectively. The spectra consist of peaks which are assigned to carbon (284 eV) and oxygen (532 eV). The atomic fractions of carbon and oxygen are determined from the intensities of the C 1s and O 1s peaks, as a function of exposing

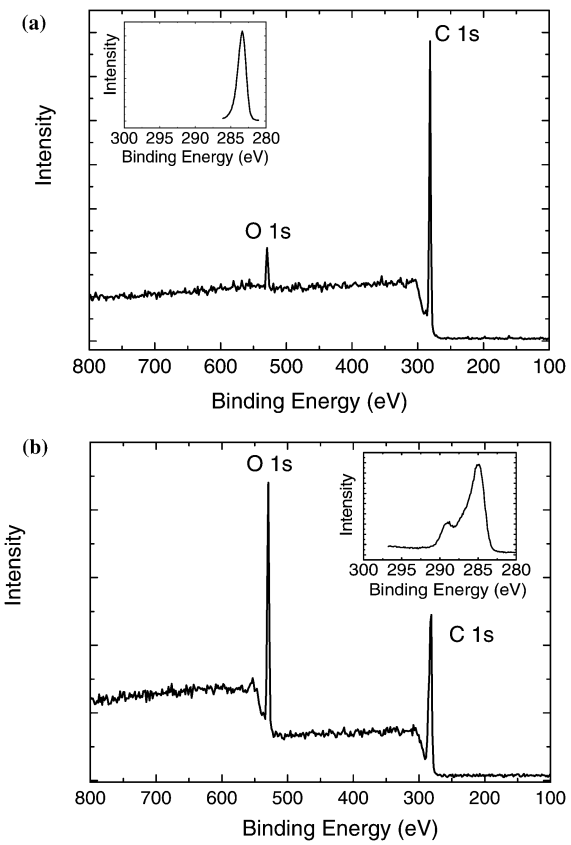

Fig. 4 XPS spectra of the honeycomb structured films before (a) and after (b) UV irradiation. The core level scans of carbon are shown in the insets.

time. Generally, the detecting depth of XPS is less than 10 nm, which offers the chemical composition on the top film surface. In the un-crosslinked film (Fig. 4a), the atomic fraction of oxygen is *ca.* 5%, suggesting trace amount of pollutant on the film surface. The core level scan of carbon in the inset of Fig. 4a shows a single and intense peak at 284 eV indicative of the sole existence of alkyl carbon (–C–C–) on top surface. After 1 h irradiation (Fig. 4b), the peak intensity at 532 eV significantly improves, corresponding to 40% oxygen atomic fraction. In the core level scan of carbon as shown in the inset, broad shoulder peaks appear at 287 and 289 eV, indicating the formation of polar groups containing oxygen as illustrated in Scheme 1 and 2.

The films cast from 12, 25 and 60 mg mL^{-1} solutions and exposed in UV for 1 h are shown in Fig. 5a–c, respectively. Either ordered porous structure or network or bimodal size distribution features are well maintained. Compared with the as-prepared films, the walls of pores in the crosslinked films become slightly thinner because of partial photo-degradation of SBS during the UV irradiation. Especially, the inner connectivity in the network structures is further revealed after the removing surface skin by UV exposure, as shown in Fig. 5b.

Another beneficial effect of the photo-chemical reaction is the formation of polar groups on the film surface, which changes surface wettability from hydrophobicity to hydrophilicity. Before UV irradiation, water droplet placed on the honeycomb structured film does not penetrate into the voids and has a stable contact angle (CA) of 118°, larger than the CA of 82° on the flat SBS film (Fig. 6a). The volume of the droplet does not change over time. The increased hydrophobicity on the porous film is attributed to the topography of the surface. According to the Wenzel model,[28] the hydrophilicity of a hydrophilic surface and the hydrophobicity of a hydrophobic surface are enhanced as the surface roughness increases. After cross-linking, the honeycomb film becomes hydrophilic due to the introduction of polar groups on the surface. Its CA is as small as 30°. Furthermore, the volume of the water droplet shrinks, accompanied with a further decrease in contact angle to about 10° within 20 s, after the initial placement of the water droplet on the honeycomb film (Fig. 6b). This indicates that the water penetrates into the micro-porous structures by capillary force. The surface wettability changing from hydrophobicity to hydrophilicity is the coordination of the introduced polar groups and the preserved honeycomb structures after UV irradiation.

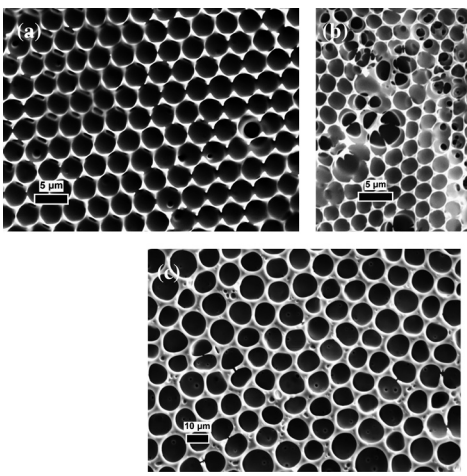

Fig. 5 Scanning electron micrographs of the micro-patterned film surface after UV irradiation for 1 h. The casting solution concentrations are (a) 12 mg mL^{-1}; (b) 25 mg mL^{-1} and (c) 62 mg mL^{-1}.

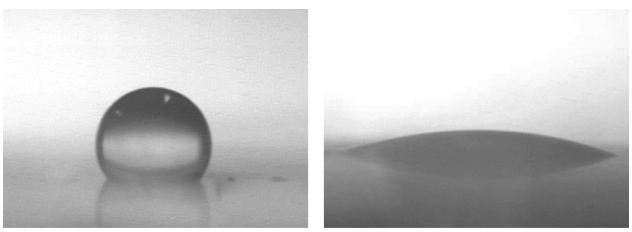

Fig. 6 Photographs of water droplets placed on honeycomb structured films before UV irradiation (a) and after 1 h UV irradiation (b).

Thermal stability and solvent resistance

The thermal resistance of the cross-linked films is characterized by heating the films up to 350 °C with a programmed temperature in air. When heated up to 100 °C (the glass transition temperature, T_g, of the PS matrix), the honeycomb structures in the as-prepared films begin to melt, collapse and totally disappear at 130 °C, observed by optical microscope (OM). However, *in situ* OM observation shows that the cross-linked honeycomb films are stable up to 350 °C, though the film color turns into deep yellow due to the thermal oxidation at high temperature. Since the OM observation gives little information about the 3-dimensional structures, the SEM is used to assess the structures after thermal treatment. The films casting from 12, 25 and 60 mg mL^{-1} solutions are cross-linked, thermally treated, imaged by SEM and shown in Fig. 7 a–c.

As discussed above, single layer of pores is formed in the films casting from 12 and 60 mg mL^{-1} solutions, local network and inter-connectivity are found in the film casting from a 25 mg

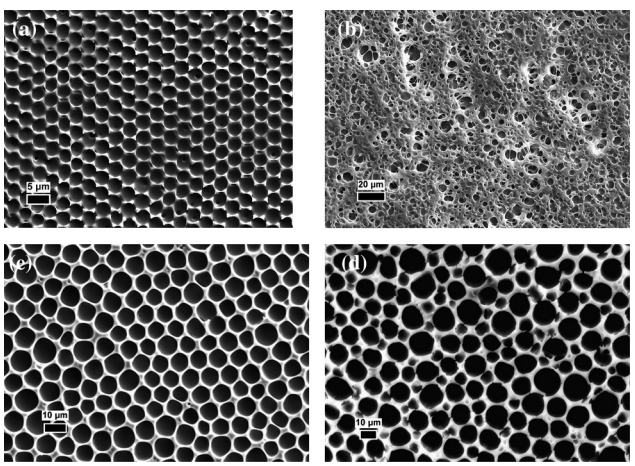

Fig. 7 Scanning electron micrographs of the micro-patterned films surface after UV irradiation for 1 h and thermal treatment up to 350 °C. The casting solution concentrations are (a) 12 mg mL^{-1}; (b) 25 mg mL^{-1} and (c) 62 mg mL^{-1}. (d) Scanning electron micrograph of the micro-patterned films surface after UV irradiation for 1 h and organic solvent immersion.

mL^{-1} solution. After cross-linkage and thermal treatment, the surface features of single layer of pores are well preserved (Fig. 7a and c). However, the melt and thermal degradation at high temperature make the walls even thinner compared with that in the films after UV irradiation. The same reason causes the partial collapse in the network structures as shown in Fig. 7b. The photo-chemical cross-linking improves not only the thermal stability, but also the resistance against organic solvents. Immersed in chloroform, a good solvent for both of the blocks, the as-cast film (un-crosslinked) immediately dissolves. The film with 1 h irradiation, on the other hand, is stable against dissolution. OM observations show an initial slightly swelling and buckling of the honeycomb structures after immersion and evaporation of solvent, however, microporous morphology is preserved in the dried films. The SEM image of the remained micro-porous structures is shown in Fig. 7d. Using the same method, we conclude that the cross-linked film is stable against a wide variety of solvents, including chloroform, tetrahydrofuran, toluene, CS_2 and benzene.

Cell morphology

It has been reported that either surface chemistry or topographic features of micro-patterned films has significant influence on cell growth and spread.[9] The combination of breath-figure method with sequent UV irradiation offers a facile method to prepare micro-patterned polymer films with adjustable surface properties. In order to investigate the influence of surface wettability and topography on cell adhesion and growth behaviours, the A549 cells are cultured up to 24 h on different substrates, including commercially available culture dish, smooth SBS film, micro-patterned SBS film and micro-patterned SBS film exposed in UV light for 1 h. After 2 h seeding, the cell number is accounted and listed in Table 1.

As mentioned in ref. 9, hydrophobic and smooth polymer surface is unfavourable for the cell attachment. We find that there are significantly fewer number of the A549 cells on the flat SBS film surface than that on the other three substrates after 2 h culture. The cell density on the honeycomb SBS film surface is equivalent to that on the culture dish (Fig. 8a and b). It is believed that a micro-patterned surface with enlarged surface area assists and enhances cell contact so that the adhesion of cells onto substrate is improved. After UV irradiation, the polar groups are introduced onto the film surface, which changes the surface wettability from hydrophobicity to hydrophilicity as discussed above. The improvement of surface wettability plus micro-patterned surface causes the best cell attachment so that the cell density achieves highest on this substrate (Fig. 8c).

Table 1 A549 cells on flat SBS film, honeycomb SBS film, culture disk and honeycomb SBS film after 1 h cross-linking

Sample	Structure	2 h (cell per cm^2)
Flat SBS film	Flat	4 300
Honeycomb SBS film	Pore size ≈ 3 μm	13 000
Culture disk	Flat	13 500
Honeycomb film after 1 h cross-linking	Pore size ≈ 3 μm	33 700

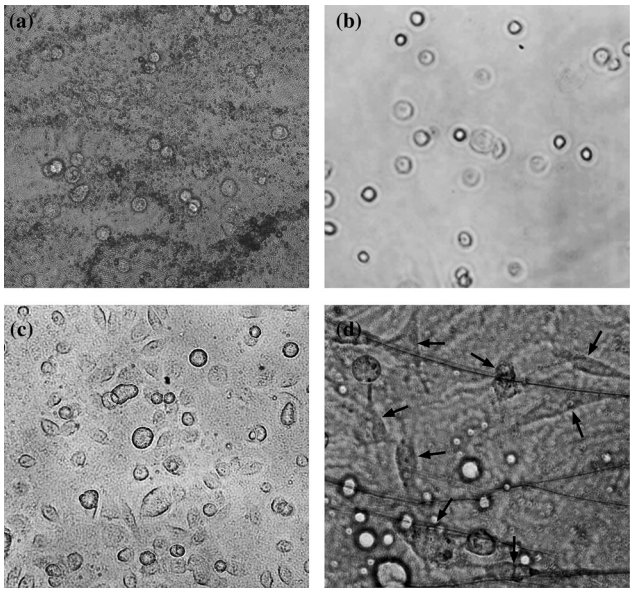

Fig. 8 Optical micrographs of A549 cells attached on different substrates after 2 h culture. (a) Honeycomb SBS film; (b) culture dish and (c) honeycomb SBS film after 1 h cross-linking. Optical micrograph of A549 cells attached on hydrophilic micro-patterned polymer film after 24 h culture is shown in (d).

Additionally, the cells on the hydrophilic micro-patterned substrate are spread much more than that on either honeycomb SBS film or culture dish. This result demonstrates that hydrophilic micro-patterned SBS film is the most compatible with cells among the employed substrates since cells attached to surface spread only when they are compatible with the surface. With extending the culture time to 24 h, the cell density on the hydrophilic micro-patterned substrate is further improved and more than that on the culture dish. Moreover, most of the cells, as pointed by the arrows in Fig. 8d, appeared to be elongating. In a further cell viability essay investigation by Hemocytometer counting method, no difference is found between the hydrophilic micro-patterned films and culture dishes, indicative of their potential cell scaffold application.

Besides surface chemistry and features, the size of patterns has also influence on the cell growth. Lee *et al.* observed that cell adhesion and proliferation were progressively inhibited as the

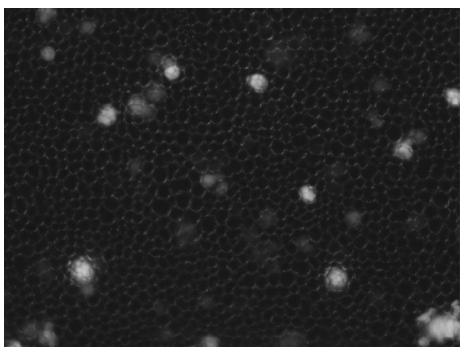

Fig. 9 Fluorescence optical micrograph of A549 cells attached on micro-patterned SBS film with bimodal size distribution.

polycarbonate membrane surfaces had micro-pores with increasing size, probably due to surface discontinuity produced by track-etched micro-pores.[29] As discussed above, dense cells with spindle-shape are found on the hydrophilic micro-patterned film surface having an average pore size of 3 μm after 2 h culture. However, in another hydrophilic micro-patterned film with main structures of 10 μm pores, only sparse cells with spherical shape are found. A fluorescence microscope observation clearly shows that the cells selectively attach into the satellite holes (Fig. 9). It seems that cells can not override the larger surface discontinuity and the cell spread is inhibited.

Conclusion

Honeycomb structured polymeric films have been prepared using a commercially available triblock copolymer with breath-figure method. By changing the solution concentration, a variety of topographic morphologies, including uniform pores, network and bimodal size distribution pores are formed. After UV irradiation, polymer films are effectively cross-linked without deforming the honeycomb structures. Either solvent resistance or thermal stability is significantly improved. In addition, the surface wettability becomes hydrophilic due to the introduction of polar groups during the UV exposure. It is found that both surface chemistry and pattern size play important roles in the cell growth. The cell adhesion and spread on the hydrophilic honeycomb surface having a pore size close to 3 μm are better than that on a commercially available culture dish.

Acknowledgements

L. Li gratefully acknowledges the National Natural Science Foundation of China (no. 50703032) and the Program for New Century Excellent Talents of Ministry of Education of China. This research was partially supported by NSFC grants (no. 30701003) and Natural Science Foundation of Fujian Province of China (no. C0710044).

References

1 T. G. Kooten, H. T. Spijker and H. J. Busscher, *Biomaterials*, 2004, **25**, 1735.
2 S. G. Zhang, *Nat. Biotechnol.*, 2003, **21**, 1171.
3 A. W. Eckert, D. Grobe and U. Rothe, *Biomaterials*, 2000, **21**, 441.
4 Y. Iwasaki, S. Uchiyama, K. Kurita, N. Morimoto and N. Nakabayashi, *Biomaterials*, 2002, **23**, 3421.
5 (*a*) E. K. Yim, R. M. Reano, S. W. Pang, A. F. Yee, C. S. Chen and K. W. Leong, *Biomaterials*, 2005, **26**, 5405; (*b*) Y. Li, W. P. Cai and G. T. Duan, *Chem. Mater.*, 2008, **20**, 615; (*c*) Y. Li, W. P. Cai, B. Q. Cao, G. T. Duan, C. C. Li, F. Q. Sun and Haibo Zeng, *J. Mater. Chem.*, 2006, **16**, 609.
6 A. S. Andersson, P. Olsson, U. Lidberg and D. Sutherland, *Exp. Cell Res.*, 2003, **288**, 177.
7 A. I. Teixeira, G. A. Abrams, P. J. Bertics, C. J. Murphy and P. F. Nealey, *Cell Sci.*, 2003, **116**, 1881.
8 C. H. Choi, S. H. Hagvall, B. M. Wu, J. C. Dunn and R. E. Beygui, *Biomaterials*, 2007, **28**, 1672.
9 Y. Ito, *Biomaterials*, 1995, **20**, 2333.
10 K. H. Kim, J. S. Cho, D. J. Choi and S. K. Koh, *Nucl. Instrum. Methods B*, 2001, **175**, 542.
11 H. Tsuji, H. Satoh, S. Ikeda, S. Ikemura, Y. Gotoh and J. Ishikawa, *Nucl. Instrum. Methods B*, 1999, **148**, 1136.
12 J. T. Groves, L. K. Mahal and C. R. Bertozzi, *Langmuir*, 2001, **17**, 5129.
13 E. Detrait, J. B. Lhoest, B. Knoops and P. Bertrand, *J. Neurosci. Method*, 1998, **84**, 193.
14 J. B. Recknor, D. S. Sakaguchi and S. K. Mallapragada, *Biomaterials*, 2006, **27**, 4098.
15 (*a*) G. Widawski, M. Rawieso and B. François, *Nature*, 1994, **369**, 387; (*b*) T. Hayakawa and S. Horiuchi, *Angew. Chem., Int. Ed.*, 2003, **42**, 2285; (*c*) J. S. Park, S. H. Lee, T. H. Han and S. O. Kim, *Adv. Funct. Mater.*, 2007, **17**, 2315; (*d*) C. X. Cheng, Y. Tian, Y. Q. Shi, R. P. Tang and F. Xi, *Macromol. Rapid Commun.*, 2005, **26**, 1266.
16 Y. Zhang and C. Wang, *Adv. Mater.*, 2007, **19**, 913.
17 T. Nishikawa, K. Arai, J. Hayashi, M. Hara and M. Shimomura, *Mater. Res. Soc. Symp. Proc.*, 2002, **724**, 229.
18 D. Beattie, K. H. Wong, C. Williams, L. A. Poole-Warren, T. P. Davis, C. B. Kowollik and M. H. Stenzel, *Biomacromolecules*, 2006, **7**, 1072.
19 U. H. F. Bunz, *Adv. Mater.*, 2006, **18**, 973.
20 B. Rånby and J. F. Rabek, *Photodegradation, Photo-Oxidation and Photostabilization of Polymers*, Wiley, New York, 1975.
21 S. F. Li, W. Dong and Y. W. Zong, *Molecular Therapy*, 2007, **15**, 515.
22 M. H. Stenzel, C. B. Kowollik and T. P. Davis, *J. Polym. Sci., Part A: Polym. Chem.*, 2006, **44**, 2363.
23 Y. Tian, S. Liu, H. Y. Ding, L. H. Wang, B. Q. Liu and Y. Q. Shi, *Polymer*, 2007, **48**, 2338.
24 D. Beysens, A. Steyer, P. Guenoun, D. Fritter and C. M. Knobler, *Phase Transitions*, 1991, **31**, 219.
25 L. L. Erdogan, J. N. Song, J. O. Wilson, M. Park and U. H. Bunz, *J. Am. Chem. Soc.*, 2004, **126**, 3678.
26 H. Yabu, M. Kojima, M. Tsubouchi, S. Onoue, M. Sugitani and M. Shimomura, *Colloids Surf. A*, 2006, **254**, 284.
27 L. Li, A. J. Zhang, C. K. Chen, X. Y. Liu, K. Cui, J. Huang, Z. Ma and Z. H. Han, *J. Colloid Interf. Sci.*, 2009, **331**, 446.
28 R. N. Wenzel, *J. Phys. Colloid Chem.*, 1949, **53**, 1466.
29 S. J. Lee, J. S. Choi, K. S. Park, G. Khang, Y. M. Lee and H. B. Lee, *Biomaterials*, 2004, **25**, 4699.

